Pulsed-laser-stimulated field ion emission from metal and semiconductor surfaces: A time-of-flight study of the formation of atomic, molecular, and cluster ions

T. T. Tsong
Physics Department, The Pennsylvania State University, University Park, Pennsylvania 16802
(Received 22 May 1984)

In field ion emission, ions are formed beyond a critical distance from the emitter surface. This distance is imposed by the condition that the energy level of the tunneling atomic electron must line up with a vacant electronic state in the solid. As a result the field-emitted ions exhibit a critical energy deficit in the energy distribution. The critical energy deficit is related to the binding energy and the ionization energy of the emitted atoms, and the work function or the electron affinity of the emitter surface. A time-of-flight measurement of the ion energy distribution and the critical energy deficit of various types of ions from both metal and semiconductor surfaces has been made using the pulsed-laser atom probe. From the result mechanisms of the formation of various types of ions in pulsed-laser-stimulated field ion emission, including novel molecular and cluster ions such as D_3^+, N_2H^+, ArH^+, $RhHe^{2+}$, $PtHe^{2+}$, $PtHe_2^{2+}$, $Si_{1\text{ to }11}^{2+}$, $Si_{1\text{ to }6}^{+}$, etc., are investigated. It is found that photoexcitation plays an important role in pulsed-laser field evaporation of silicon. Pulsed-laser field evaporation of Si can be sustained almost indefinitely by a field-gradient- and temperature-pulse-induced surface diffusion of Si atoms from the emitter shank. The most abundant Si-cluster ions are Si_4^{2+}, Si_5^{2+}, and Si_6^{2+}. These clusters and Si_{13}^{4+} are the only small, symmetrically structured atomic units one can remove from a Si crystal. The numbers 4, 5, 6, and 13 are the magic numbers in Si-cluster formation. The critical number is found to be 3 for 2+ ions. The higher ionization energies of heavy metal atoms, data of which are not readily available, can also be derived from a measurement of the critical energy deficit of field-evaporated ions.

I. INTRODUCTION

The mechanism of field ion emission,[1,2] which includes field ionization, field desorption, and field evaporation, can be directly investigated by a measurement of the ion energy distribution. Two valuable pieces of information of the ion energy distribution are the shape or the energy spread, and the critical energy deficit. The shape indicates the width of the spatial zone where the ions are formed, or the ionization probability of the ensuing atoms as a function of distance from the emitter surface. In pulsed-laser-stimulated field ion emission, Tsong and Kinkus have reported a measurement of the ion energy spread of field-emitted ions from metal surfaces using time-of-flight technique.[3] In that study an absolute mass and energy calibration was not yet achieved in our pulsed-laser time-of-flight atom probe. Thus the critical energy deficit, which is directly related to the energies of ion formation, was not obtained directly. Recently, we have succeeded in devising methods for a precision measurement of the absolute mass and energy of field-emitted ions using the pulsed-laser time-of-flight atom probe.[4] We present here results of a measurement of the ion energy distribution of pulsed-laser field-emitted atomic, molecular, and multiatomic cluster ions from both metal and semiconductor surfaces. In this study we focus our attention especially on a possible photoexcitation effect in pulsed-laser field ion emission. As will be clear from further discussion, clear evidence of a photoexcitation effect has been found in this study in pulsed-laser field evaporation of silicon.

Let us briefly discuss here why field-emitted ions should exhibit a critical energy deficit. An ion can be formed if one of the atomic electrons tunnels into the solid and is accommodated into a vacant electronic state in the solid. At low temperatures the energy level of the atomic electron must be above the Fermi level for a metal emitter and above the conduction-band edge for a semiconductor emitter. This condition imposes a critical distance x_c between the atom and the surface below which no ion can be formed. Therefore the most energetic ions of charge ne have an energy $\Delta E_n^{(n)}$ less than the full energy neV_0 of the acceleration voltage V_0. $\Delta E_c^{(n)}$ is usually called the critical energy deficit of these ions. Sometimes a slightly different term, the appearance energy,[5] is also used, which is simply given by $\Delta E_c^{(n)}+n\phi$, where ϕ is the work function of the surface. As the critical energy deficit is directly related to the energetics of ion formation, it should provide valuable insight into how some of the novel ions are formed. These ions include D_3^+, $RhHe^{2+}$, $PtHe^{2+}$, ArH^+, and atomic and cluster ions of Si. This energy is also related to the ionization energies of the emitted atoms. High ionization energies of refractory metal atoms are not readily available. It is possible that these energies can be derived from a measurement of the critical energy deficit, as will be further discussed later. Formation of cluster ions is also of great current interest. Here the formation of cluster ions in pulsed-laser field evaporation of silicon will also be discussed.

 ©1984 The American Physical Society

II. EXPERIMENTAL PROCEDURES

A. Instrumental aspects

The instrument used in this experiment is the linear-type, high-resolution pulsed-laser time-of-flight atom probe[6] shown in Fig. 1. A few essential changes from the original designs have been made for this investigation. The system now uses 300-ps laser pulses from a nitrogen laser for fast, pulsed field desorption. For the time measurement, a LeCroy model 4208 digital electronic timer with a time resolution of 1 ns is used. This timer can record up to eight flight times in one single trigger. To measure the ion energy accurately, once the ions leave the short acceleration region, they must not be subjected to any other electric fields during their flight to the detector. Such fields may make the determination of the ion energies untractable. We therefore do not use an einzel lens for focusing the ion beam in this experiment. The einzel-lens voltage can change the flight time by $\sim 1\%$, enough to completely ruin the accuracy of all of the measurements. The front face of the ion detector, a Chevron channel plate, is also grounded, and all the high-voltage connecting wires of the Chevron channel plate are carefully shielded by a grounded plate as well. Since there is no focusing of the ion beam, when using a 40-mm-diam the Chevron ion detector, the ion-acceptance angle is only $\sim 0.5°$ when a flight tube ~ 420 cm long is used. This covers a circular area at the emitter surface of 1—3 atomic diameters when the emitter voltage is varied from 3 to 10 kV. With such a small surface area covered by the ion detector, the number of ions which can be collected at a given emitter voltage in field evaporation is very small, especially if the tip voltage is low. Although the mass and energy resolution of the system is much better at low emitter voltages, field-evaporation data are usually taken around 9—12 kV. At these voltages a few hundred ions can be collected without readjusting the emitter voltage. This number is sufficient to provide an ion energy distribution with a well-defined onset flight time t_0, which is the flight time of the most energetic ions to reach the detector by the shortest flight path. The critical energy deficit of the ions can be calculated directly from the onset flight time.

To achieve a 1 part in 10 000 or 20 000 resolution in ion energy and mass measurement, the high-voltage power supply must have a stability much better than one part in 20 000, and the voltmeter must have the stability as well as the resolution. We use a digital voltmeter (DVM) of $5\frac{1}{2}$-digit resolution and a dc power supply of 0.001% stability. The overall stability of the system is checked by measuring the onset flight times of pulsed-laser field-desorbed N_2^+ and Ar^+ ions at different times and days under identical experimental conditions. We find that the onset flight times from these experimental runs agree with each other to within ± 1 ns out of a total flight time of 12 000—24 000 ns.

Two kinds of system energy resolution must be considered here. In an accurate measurement of the onset flight time t_0, the ion-flight-time spread produced by a variation of the ion flight path, due to the large surface area of the ion detector, is unimportant. In an accurate measurement of the energy spread of the ions, a large variation in the ion flight path must be carefully avoided by a proper focusing of the ion beam with the application of an einzel-lens voltage. Figure 2 shows an ion energy distribution of pulsed-laser field-desorbed Ne^+ obtained with a flight tube ~ 200 cm long at 3.2 kV from a tungsten surface. The full width at half maximum (FWHM) is only 2.27 eV, which is comparable to the best data reported in Ref. 3. This energy distribution, however, does not give any accuracy in the determination of the critical energy deficit because of the application of an einzel-lens voltage in the measurement. All the other data presented in this paper are taken without any einzel-lens voltage; under such conditions an ion-flight-path variation of about 5 parts in 10^5 can be expected from the 4-cm-diam Chevron channel plate detector and the 420-cm-long flight path. At 10 kV the energy resolution in the ion-energy-spread measurement amounts to 1 eV for doubly

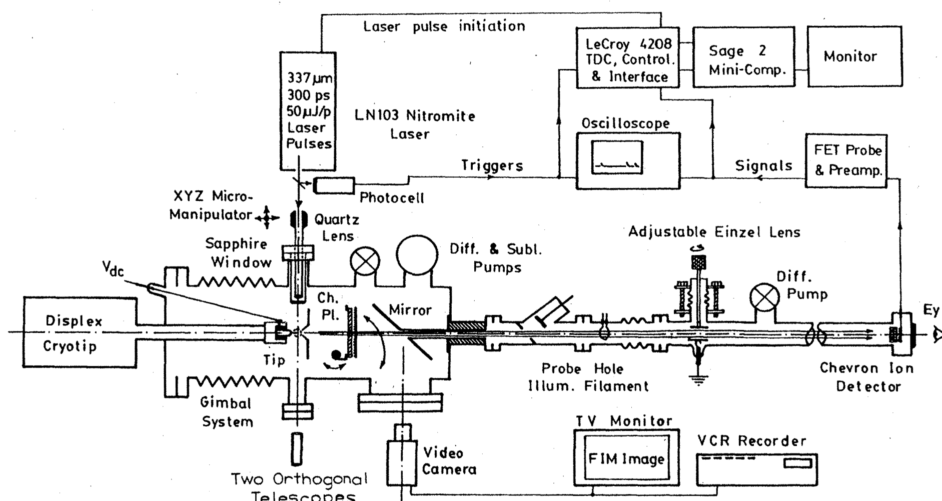

FIG. 1. Schematic diagram of the high-resolution pulsed-laser time-of-flight atom probe used in this study. The flight-path length is ~ 4207 mm. The einzel lens is grounded in this study.

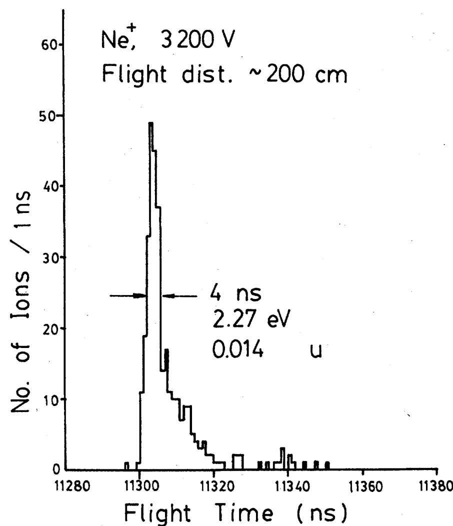

FIG. 2. The system can achieve the best resolution in ion-energy-spread measurement if a slight focusing of the ion beam is done, and if the emitter voltage is very low. Even with a flight-tube length of $\sim$200 cm, the resolution is sufficiently good to obtain a FWHM of only 2.2 eV for the pulsed-laser field-desorbed Ne^+ ions. However, to achieve the best accuracy in critical-energy-deficit measurements, no einzel-lens voltage is applied in this study.

charged ions. All the data to be presented here are optimized for the measurement of t_0, but are not optimized for the measurement of the shape of the ion energy distribution. The FWHM's of these data are usually about 3—4 eV, or wider.

If the size of the ion detector will not affect the accuracy in the measurement of t_0, a change in the flight-path length, either by a change in the room temperature or by an inaccurate emitter positioning, will. A change in the laboratory temperature by $\pm 2\,^\circ$C will change the ion flight path by $\sim\pm 3$ parts in 10^5 from the thermal expansion. An inaccuracy in the emitter positioning by 0.2 mm will change t_0 by ~ 5 parts in 10^5. Using two orthogonal telescopes and three differential screws for emitter positioning, we are able to reproduce the emitter position to ± 0.05 mm every time. However, the emitter position can change by as much as 0.5 mm by turning the refrigerator on or off. In general, taking reasonable precautions and with a keen awareness of the problem, the entire system can be managed to achieve an overall reproducibility in the measurement of the onset flight time to better than ± 1 ns, or ~ 1 part in 10^4. In some cases, a much better accuracy can be achieved by either using a reference ion species, or by repeating an experiment many times and taking the average of these measurements. We also want to point out here that since no ion-beam focusing is done, a few scattered ions are unavoidable. Thus the ion energy distributions obtained are not as "clean looking" as those taken with ion-beam focusing. Fortunately, these few scattered ions do not affect in any way the accuracy of the data and conclusions drawn.

B. Experimental methods

The kinetic energy of an ion is related to its flight time through

$$\tfrac{1}{2}mv^2=\tfrac{1}{2}m\left[\frac{l}{t+\delta}\right]^2, \tag{1}$$

where l is the flight-path length, t is the measured flight time, and δ is the triggering delay of the electronic time-measuring device which includes the trigger-pulse—generating time of the photodiode and the trigger- and ion-signal—transmission times through the connecting cables. The true flight time of the ion is $t+\delta$. In field ion emission, the most energetic ions have a kinetic energy of $neV_0-\Delta E_c^{(n)}$. Thus the onset flight-time t_0 of these ions is given by

$$\tfrac{1}{2}m\left[\frac{l_0}{t_0+\delta}\right]^2=neV_0-\Delta E_c^{(n)}, \tag{2}$$

where l_0 is the shortest flight-path distance to reach the detector. This equation is more conveniently written as

$$\frac{m}{n}=C\left[V_0-\frac{\Delta E_c^{(n)}}{ne}\right](t_0+\delta)^2 \tag{3}$$

if mass-to-charge ratios are what one is interested in. $C=2e/l_0^2$ is the flight-path constant. For our purpose here, Eq. (3) is best written as

$$\Delta E_c^{(n)}=neV_0-\frac{em}{C(t_0+\delta)^2}. \tag{4}$$

It is clear that if the values of m, C, and δ are known accurately, then the critical energy deficit of the ions can be calculated directly from the measured onset flight time.

Recently, methods for accurately determining the flight-path constant and the time-delay constant have been devised.[4] Using these methods, the value of C can be determined to an accuracy of better than a few parts in 10^5 and δ to better than 0.5 ns. In these methods, only the absolute masses of a few gaseous ions, in our case He^+, D_2^+, N_2^+, and Ar^+, and their critical energy deficits, are needed. For the values of the ion mass we take the data listed in a standard isotope table.[7] The critical energy deficit of these gas ions is taken to be $I-\phi$, where values of I are from spectroscopic data, and ϕ for tungsten high-index planes is taken to be 4.5 eV. For all the other physical parameters in the measurement, such as the flight time and emitter voltage, only a high precision in their relative values is required. The best values of C and δ for our pulsed-laser atom probe shown in Fig. 1 with the regular emitter position and the 4.2-m-long flight tube are

$$C=0.010\,828\,35\ \mathrm{u}/\mu\mathrm{s}^2/\mathrm{kV}$$
$$\delta=26.4\ \mathrm{ns}. \tag{5}$$

Some of our data are taken at another tip position. When the refrigerator is not turned on, the flight path is shorter by 0.45—0.50 mm out of a total flight path of $\sim$4207 mm. The value C has to be multiplied by a factor of $1-\Delta l/l$, and it is given by $C=0.010\,830\,6$ $\mathrm{u}/\mu\mathrm{s}^2/\mathrm{kV}$. The best accuracy can be achieved by measuring the onset flight time of heavy reference gas ions such as Ar^+, N_2^+, or Ne^+ in each experimental run and adjusting the value of C accordingly, as has been done in some of the measurements. Taking reasonable precau-

tions, the accuracy of mass and energy measurements can be achieved to a few parts of 10^5. No adjustment of δ is needed as the triggering setups are not changed in all our measurements reported here.

III. RESULT AND DISCUSSION

A. Theoretical consideration of the critical energy deficit of field-emitted ions

To facilitate the discussion of our experimental results, we will describe here why a critical energy deficit, ΔE_c, exists for field-emitted ions and what the values of ΔE_c for various types of ions are. In field ionization of gas molecules above a metal surface, Inghram and Gomer point out that ions can only be formed beyond a critical distance away from the surface.[8] This critical distance is imposed by the condition that the energy level of the atomic electron must line up with a vacant electronic state in the metal. Since all the electronic states below the Fermi level are fully occupied at low temperatures, field ionization by electron tunneling is possible only if the atomic level lines up with a vacant level above the Fermi level. The critical distance of field ionization is therefore given by

$$\int_0^{x_c} eF(x)dx \approx I - \phi \approx eFx_c \ , \tag{6}$$

where F is the applied field, I is the ionization energy of the atom, and ϕ is the work function of the surface. As a result, the maximum kinetic energy of field ions is not given by eV_0, the energy of the acceleration voltage V_0, but by $eV_0 - \Delta E_c$. ΔE_c is called the critical energy deficit and is given by

$$\Delta E_c = \int_0^{x_c} eF(x)dx \approx I - \phi \ . \tag{7}$$

In field-ionization mass spectroscopy, $I^* \equiv \Delta E_c + \phi$ is often referred to as the appearance energy of field ions.[5] The validity of Eq. (7) has already been confirmed by a large number of experimental measurements using retarding-potential methods.[9–11]

This theoretical model of field ionization above a metal surface may now be extended to field ionization above a semiconductor surface. At low temperature, all states in the valence band (VB) are occupied and all states in the conduction band (CB) are vacant. The critical distance of field ionization is now given by the condition

$$\int_0^{x_c} eF(x)dx \approx I - E_a \approx eFx_c \ , \tag{8}$$

where E_a is the electron affinity of the semiconductor surface. The critical energy deficit of field ions is then given by

$$\Delta E_c \approx I - E_a \ . \tag{9}$$

These arguments are illustrated in Figs. 3(a) and 4(a). The critical energy deficit of field ions can also be derived simply by using a conservation-of-energy argument, although in doing so no information on x_c is gained. To create a singly charged ion, an energy I is needed. Since the electron formed is accommodated into a vacant state at the Fermi level (or at the conduction-band edge), an energy of ϕ (or E_a) is gained. The minimum energy needed to form an ion near a metal (or semiconductor) surface is therefore $I - \phi$ (or $I - E_a$). This is the critical energy deficit of the ions. This simple argument is especially useful for finding the critical energy deficit of field-evaporated, multiply charged ions as well as cluster ions. The validity of this simple argument is supported by the agreement between the experimental data and the theoretical values.

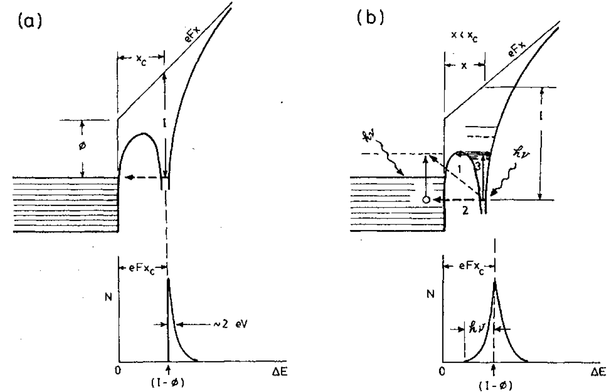

FIG. 3. (a) Potential-energy diagram for an electron in field ionization above a metal surface. (b) Three possible mechanisms of photoexcitation in field ion emission above a metal surface. See Sec. III A for explanation.

In the above discussion we invoke no occurrence of photoexcitation effects. As our experiment involves high-intensity laser irradiation of the surface, photoexcitation effects may occur. Photoexcitation effects in field ionization were investigated by Tsong *et al.* with an aluminum oxide emitter.[12] They found that field ion current at very low fields could be enhanced by a factor of 3–4 by irradiation of the emitter by high-intensity microsecond-width laser pulses. No such enhancement was observed with metal emitters. Several possible mech-

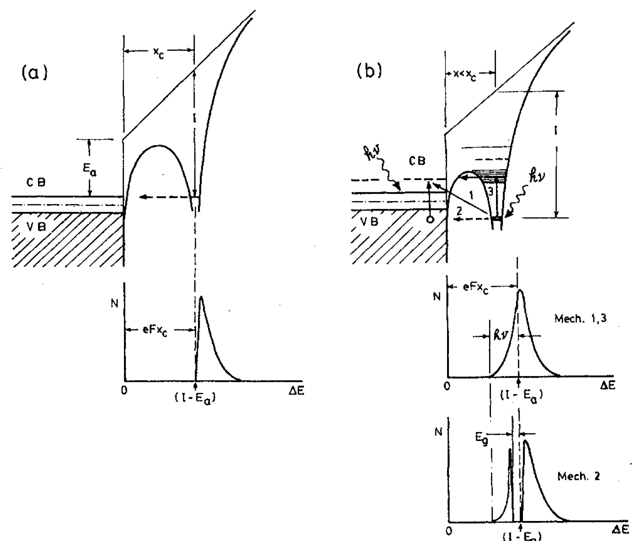

FIG. 4. (a) Field ionization above a semiconductor surface. (b) Three possible mechanisms of photoexcitation in field ion emission above a semiconductor surface. See Sec. III A for explanation.

anisms were suggested. In connection with our experimental result, to be discussed in Sec. III E, three possible mechanisms will be further pursued.

The simplest possible mechanism one can envision is that many holes are created in the valence band, or below the Fermi level, by absorption of photons, and thus the tunneling electron can now be accomodated into a vacant bulk electronic state. This mechanism is represented by path 2 in Figs. 3 and 4. Another possible mechanism is that the atom is excited to one of its excited states by resonant absorption of a photon, following by tunneling of the atomic electron into the solid. Our photon energy, 3.68 eV, is too small to excite any atom to its first excited state. However, an atom near a surface has its energy levels broadened and shifted by its interaction with the surface. The energy of photons needed to excite a surface atom may be much lower. This picture is, of course, oversimplified. The excited states of an atom, usually less than 2—4 eV below the vacuum level, are unlikely to be in pure atomic states when the atom is adsorbed on the surface. These states are more likely to be mixed states with the bulk states of the solid. Therefore the idea of resonant absorption is vague at best.

A more likely mechanism of photon-stimulated field ionization is by a direct electronic transition from the atomic state to a vacant bulk state by absorption of a photon, shown by path 1 in these figures. According to a transfer Hamiltonian theory of field ionization,[13] the electronic transition rate is given by

$$\kappa=\frac{2\pi}{\hbar}\rho_{\vec{k}}\,|\langle\vec{k}\,|\,V\,|\,a\,\rangle|^2\delta(E_{\vec{k}}-E_a)\,, \tag{10}$$

where $\rho_{\vec{k}}$ is the density of the bulk electronic states, $\langle\vec{k}\,|$ is a *vacant* bulk state, and $|\,a\,\rangle$ is the atomic state. In ordinary field ionization, even though the overlap integral increases rapidly with decreasing atom-to-surface separation, $\delta(E_{\vec{k}}-E_a)$ vanishes unless the separation is greater than x_c. Field ionization within the forbidden zone becomes possible by absorption of a photon since the δ function is now given by $\delta(E_{\vec{k}}-E_a-h\nu)$. There is probably no fine distinction between this mechanism and mechanism 3 since atomic excited states are already mixed with some bulk states. Figures 3 and 4 also show the ion energy distribution expected from the different mechanisms of photoexcitation.

In field evaporation, the situation is slightly more complicated. Field-evaporated ions are usually multiply charged. The critical distance of forming these ions depends on the detailed steps of ion formation, i.e., whether they are formed by a simultaneous transition[14] of many electrons or by step-by-step field ionization.[15] This latter process is known to be a post-field-ionization process. The critical energy deficit of these ions, however, does not depend on the detailed steps of ion formation.[3] Using the conservation-of-energy argument, one can easily arrive at the following $\Delta E_c^{(n)}$ for $n+$ metal ions:[5]

$$\Delta E_c^{(n)}=\Lambda+\sum_i^n I_i-n\phi-Q\approx\Lambda+\sum_i^n I_i-n\phi\,, \tag{11}$$

where Λ is the sublimation energy and I_i is the ith ionization energy of the atom, ϕ is the work function of the surface, and Q is the activation energy of field evaporation. Q accounts for the thermal energy of the ion at the moment it is formed. It is usually less than 0.2 eV in field evaporation. For semiconductor ions, the work function ϕ should be replaced by the electron affinity E_a. If a photoexcitation occurs in pulsed-laser-stimulated field evaporation, some changes in the energy distribution as discussed for field ionization will occur. The electronic process involved in field evaporation is very similar to that in field ionization.

Let us also consider here the critical energy deficit of cluster ions in field evaporation. In pulsed-laser field evaporation, cluster ions can be formed.[16,17] If the cluster ions are formed right at the surface, i.e., if they are not formed by fragmentation of larger clusters during their flight to the detector, then the critical energy deficit of the singly charged two-atom cluster ions can be derived from the conservation-of-energy argument to be

$$\Delta E_c(2)=2\Lambda+I'-\phi-E_b(2)-Q\approx2\Lambda+I'-\phi-E_b(2)\,, \tag{12}$$

where I' is the ionization energy of the diatomic cluster and $E_b(2)$ is the binding energy between the two cluster atoms. Equation (12) is derived by noting that an energy of $2\Lambda-E_b(2)$ is needed to remove two atoms from the solid in the form of a neutral diatomic cluster. By the same token, the critical energy deficit of n-fold, charged, m-atom cluster ions is given by

$$\Delta E_c^n(m)=m\Lambda+\sum_i^n I_i'-n\phi-E_b(m)\,, \tag{13}$$

where $E_b(m)$ is the total binding energy of the m atoms in the cluster. For the critical energy deficit of cluster ions of a semiconductor or an insulator, the same equations can still be used, except that ϕ has to be replaced by

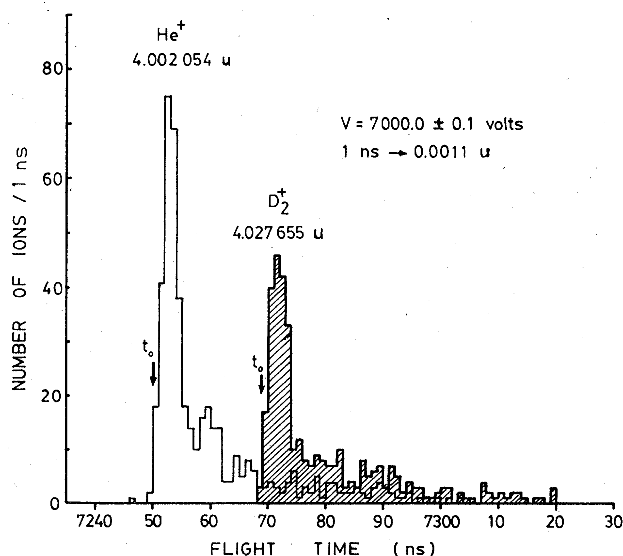

FIG. 5. Flight-time distributions of He^+ and $D_2{}^+$ plotted in a histogram of 1 ns bin width.

E_a. From these equations it is quite clear that the ionization energy of an atomic cluster can be determined from a measurement of the critical energy deficit if the cluster binding energy is known; if the ionization energy is known then the cluster binding energy can be determined. If a photoexcitation occurs in the ion formation, then the situation becomes very complicated; this case will not be dealt with here.

B. Pulsed-laser desorption of gases from metal surfaces

It has recently been shown experimentally that the difference in the critical energy deficits of pulsed-laser field-desorbed D_2^+ and He^+ ions is given by the difference of their ionization energies.[3] As can be seen from Eq. (7), this observation is consistent with the mechanism that the pulsed-laser field-desorbed ions are formed by field ionization of thermally desorbed neutrals. With the successful, accurate determination of the flight-path constant C and the time-delay constant δ of our pulsed-laser time-of-flight atom probe,[4] we are now able to directly determine the critical energy deficit of each ion species from its onset flight-time alone.

The measurement is usually done at ~ 40 K in $\sim 1\times10^{-7}$ Torr of gas at a field close to the best image field of the given gas species. With sufficient care, the flight-time distribution, or the energy distribution, of an ion species can be reproduced to within ± 1 ns, even when the data are taken several days apart. The onset flight time t_0 is taken to be the 5% peak height of the flight-time distribution, as was done in the determination of C and δ. This procedure is adapted to avoid a few scattered ions possibly due to mistriggering. In Fig. 5, flight-time distributions of $^4He^+$ and D_2^+ are shown. The critical energy deficits for various gas ions calculated from Eq. (4) using the constants given in Eq. (5) are listed in Table I. These experimental values agree with Eq. (7) within the

TABLE I. Critical energy deficits of gas ions calculated from the measured t_0 (4.2-m-long flight tube) with $\delta=26.4$ ns, $C=0.010\,828\,35$ u/μs^2/kV.

Ionic species Ionic mass (u)	V (kV)	t_0 (μs)	Measured ΔE_c (eV)	$I-\phi$ (eV)	Difference (eV)
He^+	7.0	7.250	19.5	20.1	-0.2 ± 0.3
4.002 054	7.5	7.003	20.3		
	8.0	6.779	19.8		
			(Average: 19.9 ± 0.3)		
D_2^+	2.8	11.523	11.5	11.0	0.2 ± 1.0
4.027 655	3.0	11.130	11.6		
	3.3	10.609	11.6		
	3.7	10.015	11.1		
	4.2	9.398	12.2		
	4.5	9.078	12.7		
	5.8	7.989	10.5		
	6.4	7.604	11.6		
	6.7	7.430	9.9		
	7.0	7.268	9.5		
			(Average: 11.2 ± 1.0)		
$^{20}Ne^+$	3.9	21.778	16.6	16.5	0.0 ± 0.5
19.992 439	4.2	20.980	15.9		
	6.0	17.540	16.9		
	7.0	16.233	16.4		
	8.0	15.180	15.7		
	9.0	14.310	17.2		
			(Average: 16.5 ± 0.5)		
N_2^+	4.5	23.978	11.5	11.3	-0.3 ± 0.6
28.005 599	5.0	22.743	11.4		
	6.0	20.753	10.1		
			(Average: 11.0 ± 0.6)		
Ar^+	2.8	36.352	11.3	11.3	-0.3 ± 0.7
39.961 834	3.0	35.112	11.1		
	3.3	33.474	11.6		
	4.5	28.648	11.6		
	5.0	27.170	10.5		
	6.0	24.794	9.5		
	7.0	22.953	11.2		
			(Average: 11.0 ± 0.7)		

statistical uncertainties for all the ion species. This agreement and the overall consistency of the data analysis strongly support the mechanism of pulsed-laser field desorption of gaseous ions suggested earlier,[3] i.e., by field ionization beyond x_c of the thermally desorbed neutrals. Both the shape and critical energy deficit of the energy distribution of pulsed-laser field-desorbed gaseous ions are identical to those in field ionization. We therefore conclude that there is no observable photoexcitation effect in pulsed-laser field desorption of gaseous ions from metal surfaces. In Sec. III E explanations will be given as to why photoexcitation is unlikely to occur in this case.

C. Pulsed-laser field evaporation of metals

The difficulty of accurately measuring the critical energy deficit of field-evaporated ions is that at a given applied voltage the number of ions which can be collected, within the angular extension of the Chevron detector, before the emitter radius changes significantly, is very small. A few hundred ions can be collected only if the emitter voltage is above 10 kV. The energy resolution of the system deteriorates with increasing emitter voltage since the flight time becomes shorter. Despite this difficulty, we have been able to derive reliable values of the critical energy deficit for multiply charged ions directly from their onset flight times. Results of this study are listed in Table II, and mass spectra of $^{56}Fe^{2+}$ and Pt^{2+} ions are shown in Figs. 6 and 7. These values of ΔE_c agree with Eq. (11) within the experimental uncertainties given.

As has been pointed out earlier, a slight change in the room temperature or tip position will produce an appreciable change in the flight-path constant C. The accuracy of the measurement of ΔE_c for multiply charged ions can be greatly improved if an energy distribution of a gas-ion species of comparable mass-to-charge ratio can be collected from the same field ion emitter preferably at the same tip voltage and collected on the same day. Using this gas-ion data the value of C can be adjusted to exactly the same physical conditions where the energy distribution of metal ions is collected. An example of this procedure is shown in Fig. 8 for N_2^+ and $^{56}Fe^{2+}$ ions. Using this method the critical energy deficit of $^{56}Fe^{2+}$ is found to be $\Delta E_c^{(2)} = (10.2 \pm 0.5)$ eV. This value agrees with Eq. (11) to within (0.4 ± 0.5) eV. When this method is used, an emitter voltage should be chosen such that the difference in the onset flight times of the two species is large. Figure 9 shows the expected flight-time differences between N_2^+ and $^{56}Fe^{2+}$, between N_2^+ and $^{28}Si^+$ as functions of emitter voltages. A few experimental points available are also included. At very low emitter voltages, the flight-time differences are usually larger. Unfortunately, it is difficult to collect a sufficient number of ions at a low emitter voltage, and a compromise has to be made.

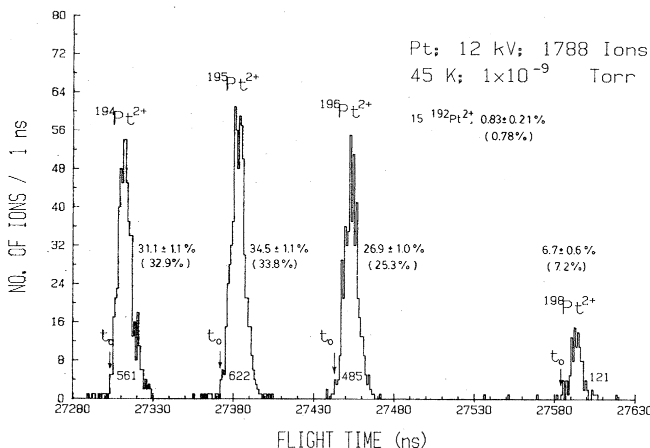

FIG. 7. Mass spectrum of Pt^{2+} and its flight-time distributions taken in vacuum. Values of t_0 are listed in Table II.

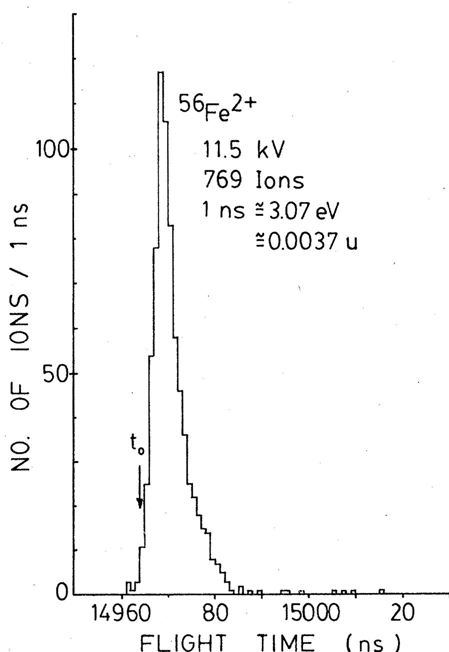

FIG. 6. Flight-time distribution of field-evaporated $^{56}Fe^{2+}$ ions take in vacuum. $t_0 = 14\,964$ ns.

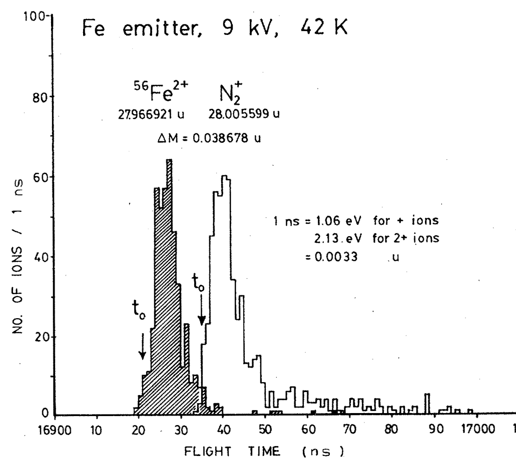

FIG. 8. $^{56}Fe^{2+}$-N_2^+ doublet in mass spectroscopy. Their onset flight times are separated by 14 ns.

The critical energy deficits of metal ions measured in this study are listed in Table II. These values agree with Eq. (11) to within the statistical uncertainties of the data, thus confirming the validity of this equation. Obviously, the critical-energy-deficit data can be used to determine the higher ionization energies of metal atoms. Such data are scarce. In a recent compilation of ionization energies of various elements by Moore,[18] little data are listed for ionization energies of heavy elements. The present method can be adapted for measuring these energies, although, at the present stage, the accuracy is only about 2–4 %, as can be seen from Table II. This accuracy can, of course, be greatly improved by using laser pulses of shorter duration and an electronic timer of better time resolution. Laser pulses of 1 ps width and electronic timers with a time resolution of 50 ps are now commercially available. A reliable measurement of the higher ionization energies of heavy elements can be achieved only if the energy resolution of the atom probe is improved by a factor of 10 or more by adopting these units to the system.

Our data also show no evidence of a photoexcitation effect in pulsed-laser-stimulated field evaporation from

TABLE II. Critical energy deficits of metal ions derived from the measured t_0 (4.2-m-long flight tube).

Ionic species Ionic mass (u) C (u/μs^2/kV)	V (kv)	t_0 (μs)	Measured $\Delta E_c^{(n)}/n$ (eV)	$\left[\Lambda+\sum_i^n I_i-n\phi\right]/n$ (eV)	Difference
$^{56}Fe^{2+}$	9.0	16.921	9.5	9.8	-0.3 ± 0.5
27.966 921	11.0	16.051	10.1		
$C=0.010\,830\,6$	11.5	14.964	8.8		
			(Average: 9.5 ± 0.5)		
$^{58}Ni^{2+}$	9.0	17.222	8.2	10.1	1.1 ± 0.9
28.967 125	10.0	16.336	8.1		
$^{60}Ni^{2+}$	9.0	17.518	9.7		
29.964 846	10.0	16.617	10.0		
			(Average: 9.0 ± 0.9)		
$C=0.010\,828\,35$					
Rh^{2+}	6.1	27.910	11.6	10.9	0.2 ± 0.8
51.452 201	8.7	23.357	9.9		
$C=0.010\,828\,35$	9.2	22.713	10.7		
	10.0	21.785	12.1		
			(Average: 11.1 ± 0.8)		
$^{182}W^{3+}$	12.0	21.591	14.6	15.1[a]	0.7 ± 1.0
60.648 859					
$^{183}W^{3+}$	12.0	21.652	16.3		
60.982 866					
$^{184}W^{3+}$	12.0	21.710	15.0		
61.316 435					
$^{186}W^{3+}$	12.0	21.830	17.1		
61.984 243			(Average: 15.8 ± 1.0)		
$C=0.010\,828\,35$					
$^{194}Pt^{2+}$	12.0	27.303	11.5	11.4[a]	-0.3 ± 0.6
96.980 791					
$^{195}Pt^{2+}$		27.372	10.2		
97.481 844					
$^{196}Pt^{2+}$		27.443	10.9		
97.981 925					
$^{198}Pt^{2+}$		27.584	11.7		
98.983 391			(Average: 11.1 ± 0.6)		
$C=0.010\,830\,8$					

[a]Estimated value.

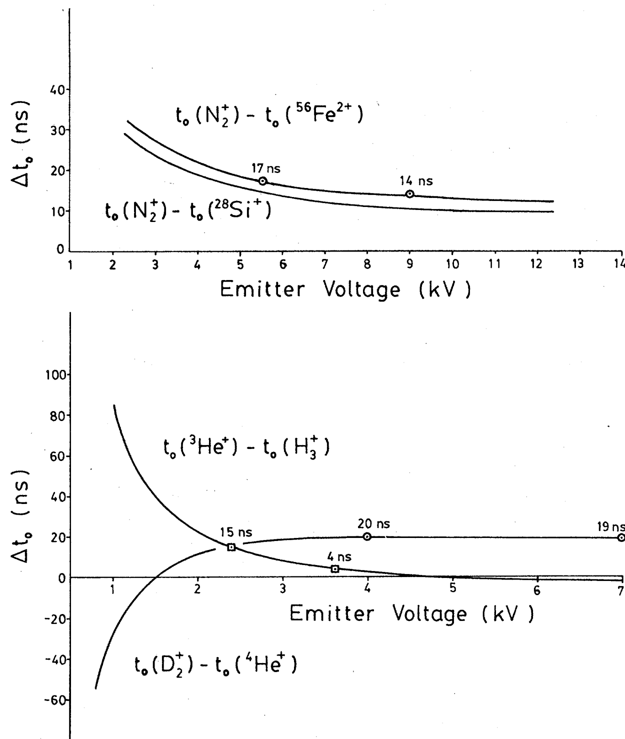

FIG. 9. Calculated flight-time differences for four mass doublets, and experimental data obtained from this and an earlier (Ref. 3) study. The agreement is always within one bin width of the data, which is 1 ns in this study and 1.25 ns in the earlier study.

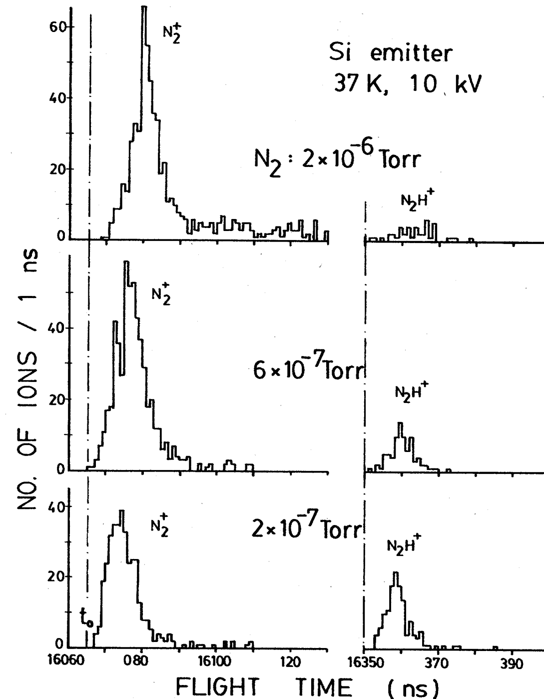

FIG. 10. Pulsed-laser field desorption of nitrogen from a silicon emitter surface. The background pressure is $\sim 1\times10^{-9}$ Torr. Note the shifting of the onset flight time t_0 of the N_2^+ ions toward higher values when the gas pressure is increased. The center line indicates the t_0 calculated from values of C and δ given in Eq. (5). Also note the formation of N_2H^+ ions. The hydrogen partial pressure must be in the 10^{-10}-Torr range.

metal surfaces since neither the critical energy deficit nor the ion energy distribution exhibits any feature of a photoexcitation effect. The same conclusion was reached by Tsong *et al.* in their search for a photoexcitation effect in field ionization.[4] In contrast, we have observed a strong photoexcitation effect in pulsed-laser-stimulated field evaporation of a semiconductor. The lack of a photoexcitation effect in field ion emission from metal surfaces will be further discussed in connection with field evaporation of silicon in Sec. III E.

D. Pulsed-laser field desorption of gases from silicon surfaces

It is found that the onset flight time of pulsed-laser field-desorbed gas ions from a silicon emitter surface depends on the gas pressure in the system. An example of this behavior is shown in Fig. 10. This behavior can be easily interpreted by the high resistivity of the silicon emitter at low temperatures. Since the dc field ion current will produce an iR drop along the silicon emitter, the voltage at the emitter surface is the applied voltage V_0 reduced by the iR drop. The true onset flight time t_0 of the applied voltage V_0 can be derived by plotting the measured onset flight time as a function of the gas pressure. As the onset flight-time change is only $\sim$4 ns when the gas pressure increases from 2×10^{-7} to 2×10^{-6} Torr, and our timer has a time resolution of only 1 ns, a meaningful plot cannot yet be obtained. However, Fig. 10 is consistent with such a behavior, and from which the true onset flight time, or the onset flight time at zero gas pressure, of N_2^+ at 10 kV, is derived to be (16066 ± 1) ns. The calculated onset flight time t_0, found by taking $\Delta E_c = I - E_a$, is 16065 ns. This calculated value agrees with the measured value to within ±1 ns. This set of data thus shows no photoexcitation effect in the pulsed-laser field desorption of N_2 from the silicon surface either.

The shape of the ion energy distribution also changes with the gas pressure, as can be seen from Fig. 10. At high gas pressure the low-energy tail is much more prominent. These low-energy ions may have resulted from a scattering effect. We have also studied pulsed-laser field desorption of Ar from silicon surfaces at 85 K, which shows a similar behavior.

In principle, the effect of iR drop can be eliminated by performing the onset-flight-time measurement at a high emitter temperature so that the resistance of the silicon emitter is greatly reduced. In practice, however, this cannot be done since Ar and N_2 cannot be pulsed-laser field-desorbed without also field-evaporating the substrate atoms when the Si emitter is kept above $\sim$100 K.

E. Pulsed-laser field evaporation of silicon: cluster-ion formation and a photoexcitation effect

Pulsed-laser field evaporation of silicon has been reported by Kellogg and Tsong.[19] Silicon field-evaporates as

atomic ions, Si^{2+} and Si^+, and cluster ions as shown in Figs. 11(a) and 11(b). The cluster ions have been identified earlier as $Si_{2\,to\,5}{}^+$, and $Si_3{}^{2+}$.[17] In this study we will focus on three aspects of silicon field evaporation, namely a careful identification of the cluster ions and the magic and critical numbers of Si cluster-ion formation, the ion energy distribution, and a photoexcitation effect.

To avoid the effect of the *iR* drop, all our field-evaporation studies of silicon are done in a vacuum of $\sim 6\times 10^{-10}$ to 2×10^{-9} Torr. Under this vacuum condition, *iR* drop should be negligibly small, as has already been shown in a gas-desorption experiment. A further confirmation of this point will be presented later. We find the field-evaporation behavior of silicon under high-intensity pulsed-laser irradiation to be very different from that of metals. In addition to the atomic ions Si^{2+} and Si^+, about 5—15 % of the ions are cluster ions. The abundance of cluster ions increases wth laser intensity.[17] The pulsed-laser field evaporation can be sustained almost indefinitely by adjusting the emitter voltage and laser intensity, indicating that a field-gradient- and temperature-pulse-induced surface diffusion of silicon atoms from the emitter shank to the apex occurs continuously. It appears that an equilibrium cone-shaped protrusion, generally referred to as the Taylor cone, is eventually formed on a relatively dull emitter surface. Since the pulsed-laser-stimulated field evaporation can be sustained almost indefinitely, this technique probably can be developed into a pulsed silicon-ion source for point-doping applications. For our study here, we are able to collect statistically reliable amounts of data at a relatively low emitter voltage. Several sets of data, each containing more than 2000 ions, have been collected. The data shown in Fig. 11 are taken at 6 kV and 300 K in vacuum of 1×10^{-9} Torr or lower. This set contains a little over 15 000 ions with $\sim 15\%$ of the ions are cluster ions. The mass lines, or the energy distributions of Si^{2+}, are quite sharp, and the three isotopes are completely separated as shown in Fig. 12. In contrast, isotope lines in Si^+ and cluster ions are not so well separated, as shown in Figs. 13 and 14. We attribute the energy spread of Si^+ ions as resulting from a gradual fragmentation of multiply charged cluster ions into smaller cluster ions or atomic ions by Coulomb repulsive interactions between the charges; this is known as Coulomb explosion.[20] Although the main peak of Si^+-ion energy distribution is sharper than Si^{2+}, there is a very small low-energy tail which persists to over ~ 200 eV. This low-energy tail becomes more prominent if a larger fraction of cluster ions is formed. It will disappear completely if field evaporation is done at high field and very low laser intensity where few cluster ions are formed.

The identification of ionic species of the cluster ions is not as straightforward as has been reported.[17,20] For example, $Si_2{}^+$ and $Si_4{}^{2+}$ have exactly the same mass-to-charge ratio and cannot be mass-separated. Fortunately, there are three isotopes of silicon, each separated by 1 u. If the cluster ions of doubly charged, half-mass peaks should be present by a mixing of the isotopes. If the cluster ions are singly charged, then no half-mass peaks should be present. Figure 14 shows two examples. When

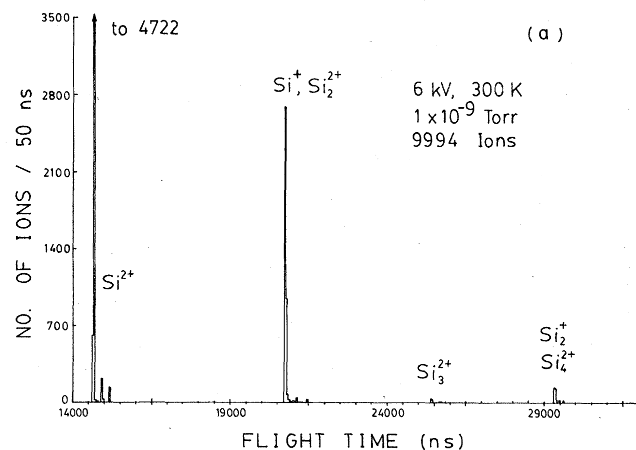

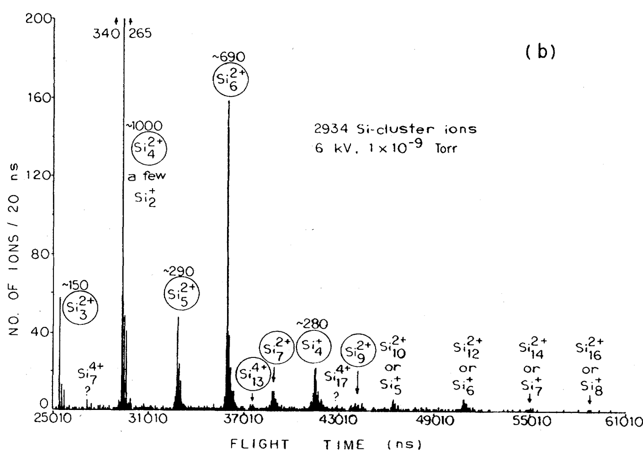

FIG. 11. (a) and (b) Complete mass spectrum of pulsed-laser field-evaporated silicon ions plotted in histograms of 50 and 20 ns bin widths. A correct identification of mass lines are discussed in the text and in Figs. 12—14. Note the fine structures which cannot be well reproduced in the print.

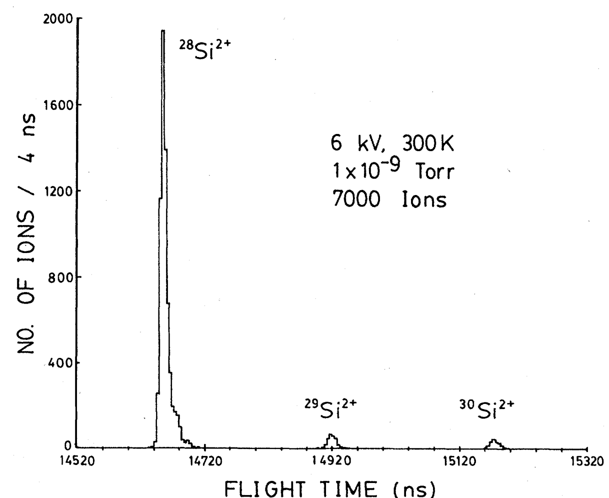

FIG. 12. Mass lines of Si^{2+}. Note the sharpness of the ion energy distribution and the absence of a low-energy tail.

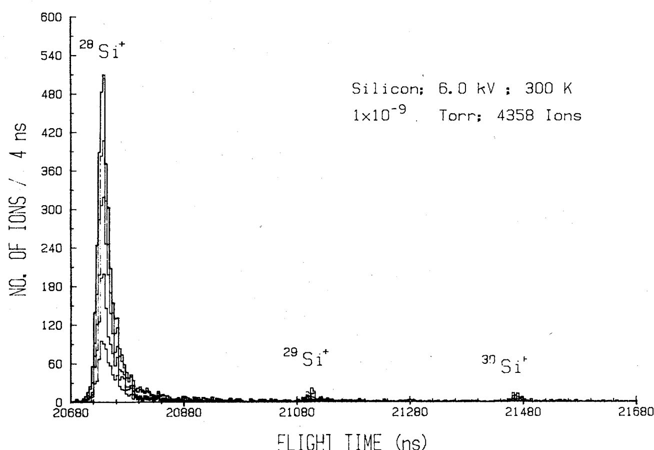

FIG. 13. Mass lines of Si^+. Although the ion energy distribution is sharp, it contains a low-energy tail which extends to more than 200 eV. These low-energy ions are produced by field dissociation of multiatomic clusters far away from the emitter surface. Note also that there are no half-integral mass lines; thus these mass lines do not contain Si_2^{2+} ions.

the flight times of the ions with m/n values of around 56 are plotted in a histogram of 10 ns bin width, half-integral mass peaks are found. The $m/n = 56.5$ mass line can only arise from 2+ ions containing three ^{28}Si and one ^{29}Si atoms. Similarly, when the flight times of the ions with m/n values of around 84 are plotted in a histogram of 10 ns bin width, half-integral mass peaks of 84.5, 85.5, 86.5, etc., are found. These peaks can arise only from Si_6^{2+} ions of various combinations of the silicon isotopes. It is interesting to note that no detectable half-integral mass peaks are present near $m/n=28$ and 112. Thus these ions are indeed Si^+ amd $Si_4{}^+$, as identified.

Let us consider here what the fractional abundances of cluster ions of various mass-to-charge ratios are. The fractional abundances of ^{28}Si, ^{29}Si, and ^{30}Si are represented, respectively, by a, b, and c. The fractional abundances of multiatomic clusters are given by the corresponding coefficients in the multinomial expansion. For example, the fractional abundance of n-atom clusters with i ^{28}Si atoms and j ^{29}Si atoms and $(n-i-j)$ ^{30}Si atoms is given by

$$[n!/i!j!(n-i-j)!]a^i b^j c^{(n-i-j)} .$$

In Table III we list the expected fractional abundances of ions of various mass-to-charge ratios for some cluster ions. It is quite obvious that, for singly charged ions, no half-integral values should be present. In principle, the relative abundance of the singly and doubly charged cluster ions for each ion species can be determined from the relative intensities of the half-integral and integral mass lines. The very small fractional abundances of ^{29}Si and ^{30}Si, and the small amount of cluster ions formed in pulsed-laser field evaporation, make such a determination unreliable. From the data shown in Fig. 11(b) and the fine structures obtained, such as those in Fig. 14, the following conclusions can be drawn. (1) Most of the cluster ions are doubly charged, although some of the heavy cluster ions cannot yet be identified because of the very small number of ions formed. A notable exception is the mass peak around $m/n \approx 112$. Its fine structure shows mass lines of $m/n = 112$, 113, and 114, etc., without the presence of half-mass lines. Thus this species is identified as $Si_4{}^+$. (2) In general, cluster species with an even number of atoms per cluster are more abundant, especially when

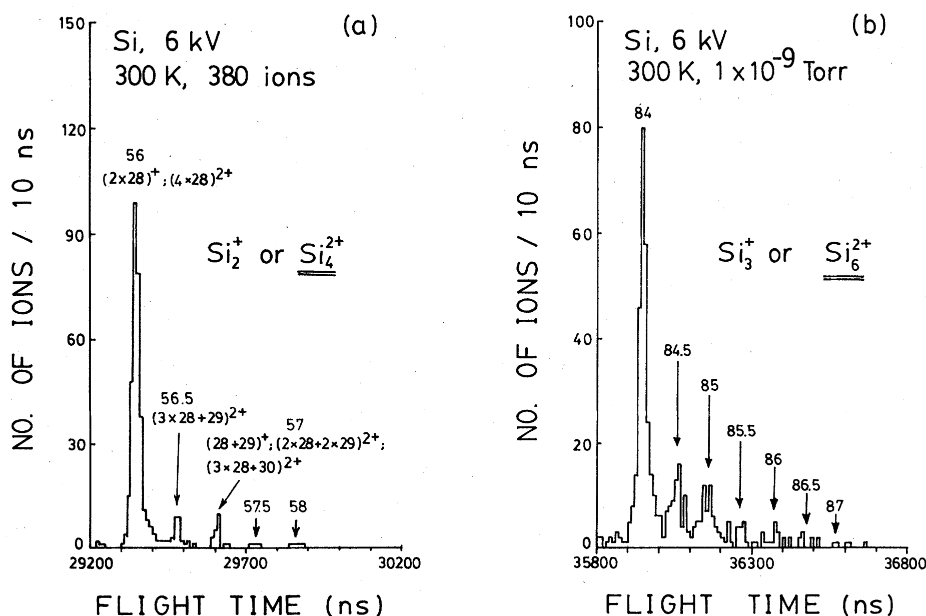

FIG. 14. (a) and (b) Identification of silicon-cluster ions. The existence of prominent half-integral mass (mass-to-charge ratio) peaks indicates that most of these ions are 2+ ions. Thus they are identified as (a) $Si_4{}^{2+}$ and (b) $Si_6{}^{2+}$. We conclude that silicon-cluster ions are dominantly doubly charged.

TABLE III. Expected fractional abundance of various cluster ions. The fractional abundances of silicon isotopes 28, 29, and 30 are, respectively, $a=92.2\%$, $b=4.7\%$, and $c=3.1\%$.

Cluster ion	Mass-to-charge ratio	Combinations	Fractional abundance (%)
Si_2^+	56	28 + 28	$a^2=85.0$
	57	28 + 29	$2ab=8.7$
	58	28 + 30, 29 + 29	$2ac+b^2=5.9$
	59	29 + 30	$2bc=0.3$
	60	30 + 30	$c^2=0.1$
Si_4^{2+}	56	4×28	$a^4=72.3$
	56.5	3×28+29	$4a^3b=14.7$
	57	2×28+2×29, 3×28+30	$6a^2b^2+4a^3c=10.8$
	57.5	2×28+29+30, 28+3×29	$12a^2bc+4ab^3=1.5$
	58	2×28+2×30, 28+2×29+30, 4×29	$6a^2c^2+12ab^2c+b^4=0.6$
	⋮		
Si_3^+	84	3×28	$a^3=78.4$
	85	2×28+29	$3a^2b=12.0$
	86	2×28+30, 28+2×29	$3a^2c+3ab^2=8.5$
	87	28+29+30, 3×29	$6abc+c^3=0.8$
	⋮		
Si_6^{2+}	84	6×28	$a^6=61.4$
	84.5	5×28+29	$6a^5b=18.8$
	85	4×28+2×29, 5×28+30	$15a^4b^2+6a^5c=14.8$
	85.5	4×28+29+30, 3×28+3×29	$30a^4bc+20a^3b^3=3.3$
	86	4×28+2×30, 2×28+4×29, 3×28+2×29+30	$15a^4c^2+15a^2b^4+60a^3b^2c=1.4$
	⋮		

the number is an integral multiple of 4. For cluster ions with an odd number of atoms, the species with five atoms is the most abundant. This cluster can be formed with the atomic structure where a Si atom has each of its four bonds bounded by another Si atom. Two of the four covalent bonds are, of course, unsaturated for a doubly charged ion. (3) The most abundant species, Si_4^{2+}, is consistent with the structure in which a Si atom has three of its bonds saturated with Si atoms and one completely broken. The second most abundant species, Si_6^{2+}, is consistent with the structure of a closed hexagonal but noncoplanar ring of the (111) bilayer having two bonds of each Si atom bound to two neighboring Si atoms. (4) A small number of 4+ cluster ions seems to exist, although only Si_{13}^{4+} can be clearly identified. The structure of this ion species is consistent with three hexagonal rings of the (111) bilayer arranged in an equilateral triangle. It is interesting to note that Si_4, Si_5, Si_6, and Si_{13} are the only highly symmetric small-atom units which can be removed from the (111) planes of a Si crystal. These numbers, 4, 5, 6 and 13, may be called magic numbers[20] in Si-cluster formation. These numbers are identified in this study from multiply charged cluster ions. Finally, one should ask the question why it is possible to observe such small doubly charged cluster ions of only *three* atoms for covalently bonded Si clusters. According to Sattler *et al.*,[20] the critical numbers for doubly charged metallic Pb_m^{2+}, ionic $(NaI)_m^{2+}$, and van der Waals Xe_m^{2+} ions are 30, 20, and 52, respectively. Below these critical numbers, Coulomb explosion can occur, and doubly charged ions are unstable. Our answer to this question is that silicon atoms do not form closely packed clusters, but rather have very open structures. This is an interesting question which merits further attention.

Another interesting finding of this study is that more than 30% of Si^+ ions and more than 50% of Si^{2+} ions in pulsed-laser-stimulated field-evaporation experiments have a smaller energy deficit than that expected from Eq. (11). We have collected several sets of data at different emitter voltages and temperatures. All of them show the same features. An example is shown in Fig. 15, where the flight times of $^{28}Si^+$ and $^{28}Si^{2+}$ are plotted in histograms of 1 ns bin width. The onset flight times, calculated from Eq. (11) by using $E_a=4.1$ eV and $\Lambda=4.64$ eV, do not fall into the 5% peak height of the leading edges of these ion energy distributions as they do in all other types of pulsed-laser field-emitted ions. In fact, the onset flight times fall slightly over the low-energy side of the peak positions. This same behavior persists even when the emitter temperature is changed from 85 to 300 K as shown in Fig. 16. As our system has a reproducibility in flight-time measurement of ± 1 ns over a long period of time, these ions, with an excess energy of several electron volts, are not an artifact of the limited resolution of the instrument, but rather are produced by a photoexcitation effect, as discussed in Sec. III A.

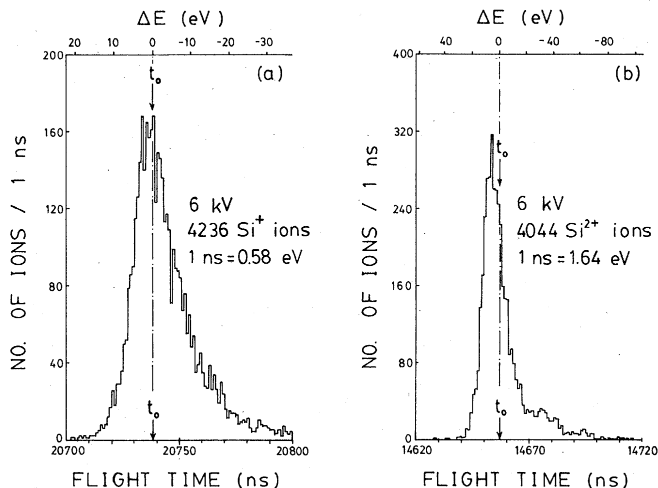

FIG. 15. (a) and (b) Energy distribution of pulsed-laser field-evaporated Si^{+} and Si^{2+} ions plotted in histograms of 1 ns bin width taken in a vacuum below 1×10^{-9} Torr. t_0 indicates where the onset flight time should be if there were no photoexcitation effect. The fact that a large fraction of the ions has energy exceeding the maximum expected energy indicates the occurrence of a photoexcitation effect in the ion formation. These distributions are reproducible to within ±1 ns in different runs taken on different days.

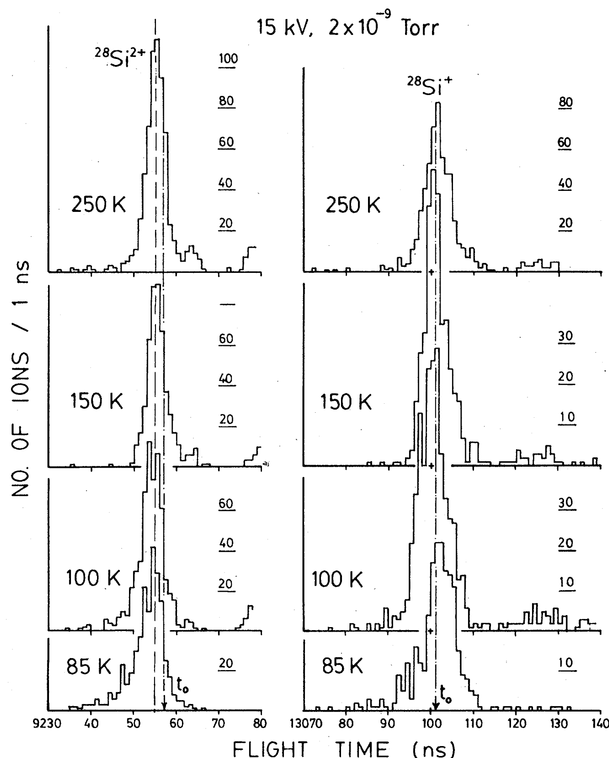

FIG. 16. Emitter temperature dependence of the energy distribution of pulsed-laser field-evaporated Si^{+} and Si^{2+} ions. Within ±1 ns bin width and the expected statistical fluctuations, no dependence on emitter temperature of the energy distributions is evident.

The question now is which of the mechanisms discussed is the viable one. As shown in Fig. 4, different mechanisms will give different energy distributions, one with two separated peaks and one with widened distribution width. Unfortunately, the energy resolution of our system probably cannot resolve the two peaks even if they exist. At 6 kV, the band gap, 1.12—1.15 eV in width, corresponds to only a 2.4-ns flight-time difference of Si^{+} ions, and a 1-ns difference of Si^{2+} ions. Since the leading edge of a field ion energy distribution is usually more than 2—3 ns in width, there is no possibility of resolving the two peaks even if they exist. It appears, however, that the direct-transition mechanism, as indicated by the arrow 1 in Fig. 4, is favored for the reason that the overlap integral increases with decreasing surface-to-atom separation. The width of the ion energy distribution is almost twice as wide as those in field ionization above a metal surface. We also want to point out here that the excess energy of many of these photoexcited ions is as large as ~8 eV, well exceeding the photon energy 3.68 eV. Thus, multiphoton excitation also seems to occur in pulsed-laser-stimulated field evaporation of silicon, as it does in most solid-state excitations. We want to point out here that field penetration and band bending at a silicon surface will not change the critical energy deficit.[21] Other effects, such as resistivity, can only reduce the ion energy. The excess energy we have observed is at least 10 times larger than the uncertainty of our atom probe in energy measurements at this tip voltage, and this is not an artifact.

It is worthwhile to try to explain why a photoexcitation effect has not been observed in pulsed-laser field evaporation of metals. In metals there is no energy band gap. Even if field ionization by photoexcitation can occur, the ion formed will be reneutralized before it can leave the surface region. The lack of a photoexcitation effect in pulsed-laser field desorption of gases from both semiconductor and metal surfaces is probably due to the fact that gas molecules have already left the surface before a photon-assisted field ionization can occur. All the explanations presented here are tentative. A detailed theory is needed to explain these experimental observations. It has been pointed out in Sec. III A that the ionization energy and binding energy of atomic clusters can be studied by measuring the critical energy deficit of these ions. Because of the complication of the photoexcitation effect, and also the very small fraction of cluster ions formed, this is not yet possible in this study.

We would also like to point out here that although the low-laser-power pulsed-laser-stimulated field evaporation of silicon seems to proceed regularly as in field evaporation of metals, as has also been observed by Kellogg,[17] it is inconceivable that the pulsed-laser-stimulated field evaporation reported here really proceeds one atomic layer by atomic layer. One cannot expect formation of large cluster ions by single-atomic-layer field evaporation. The layer-by-layer field evaporation of silicon may, in fact, proceed in multiatomic layers. For example, on the (111) layer one can expect the field evaporation, both dc and pulsed-laser assisted, to proceed two atomic layers by two atomic layers since bilayer structure exists on this plane.

The field-evaporation behavior of silicon is still poorly understood and needs to be further investigated.

IV. CRITICAL ENERGY DEFICIT OF NOVEL IONS IN PULSED-LASER FIELD ION EMISSION

In pulsed-laser field ion emission, novel ions, such as metal helides, dihelides, ArH^+, H_3^+, N_2H^+, etc., are often observed. It is interesting to measure the critical energy deficit of these novel ions, from which the bonding mechanism of these ions may be studied.

In the presence of $\sim 2\times 10^{-7}$ Torr of helium, pulsed-laser field evaporation of a platinum emitter kept at 45 K results in the formation of a large fraction of $PtHe^{2+}$ ions and a small number of $PtHe_2{}^{2+}$ ions. The fraction of helide and dihelide ions depends on the field strength at which the pulsed-laser field evaporation is carried out. At a field of $\sim$4.8 V/Å, near the dc evaporation field of Pt, more than 70% of all the field-evaporated ions are helides. This is shown in the shaded mass lines of Fig. 17. When the field is dropped to $\sim$4.3 V/Å by further field evaporation of the surface, the fraction of helides drops to $\sim$30% or less. Whenever helide ions are present in the mass spectrum, there are always a few more scattered ions. These are produced by field dissociation of helide ions into metal ions and helium ions, and possibly also neutrals. The energy distributions of $PtHe^{2+}$, plotted in a histogram of 2 ns bin width, are shown in Fig. 18. It is quite clear that the line shape of $PtHe^{2+}$ is comparable to that of Pt^{2+} in vacuum field evaporation (Fig. 7). In Table IV the critical energy deficits measured for $PtHe^{2+}$ and $RhHe^{2+}$ are shown. They are only about 0.5 eV higher than those of metal ions. This result suggests that the bonding mechanism of a metal helide ion is most probably produced by a polarization force between a metal ion and a neutral helium atom, not by formation of covalent bonds, or ionic bonds, since the bond energy is $\sim$0.5 eV.[22]

Other novel ions observed in this study are ArH^+ and N_2H^+ from a silicon surface, and D_3^+ ions from metal surfaces. Figure 19 shows a mass spectrum containing ArH^+ ions. Their critical energy deficits are also listed in Table IV. Recently, we determined the critical energy deficit of pulsed-laser field-desorbed H_3^+ by comparing the flight times of H_3^+ and $^3He^+$. In this study we are able to calculate it directly from the onset flight time of D_3^+ alone. The present result agrees with the earlier one, thus further supporting the mechanisms of H_3^+ formation proposed earlier.[3]

Finally, even though our pulsed-laser atom probe now has a resolution better than 1 part in 10 000 in ion energy and absolute ion-mass measurements, the accuracy of the critical-energy-deficit measurement is still somewhat limited because of the relatively high energy of field-emitted ions. The resolution of the system can be further im-

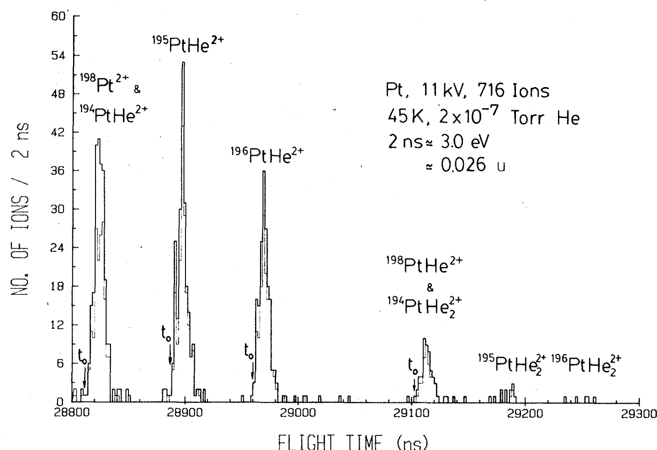

FIG. 18. Energy distributions of $PtHe^{2+}$ ions. Except for a few more scattered ions, these energy distributions are almost identical to those of the Pt^{2+} ions shown in Fig. 7.

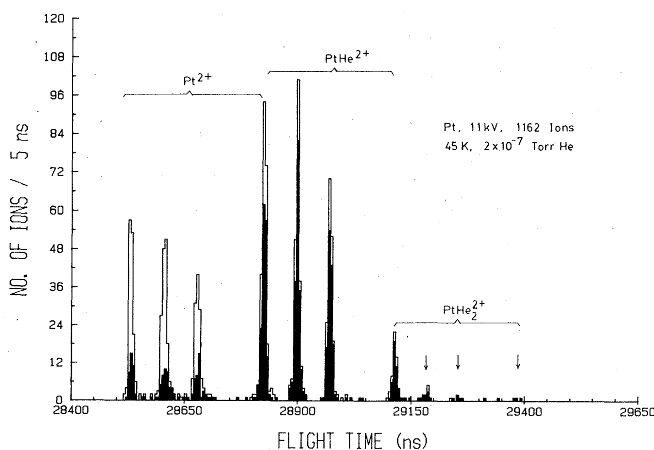

FIG. 17. Formation of $PtHe^{2+}$ and $PtHe_2{}^{2+}$ ions. Shaded part is obtained in a field between 4.8 and 4.6 V/Å and the nonshaded part between 4.6 and 4.3 V/Å. The helide ions are much more abundant when the applied field is higher.

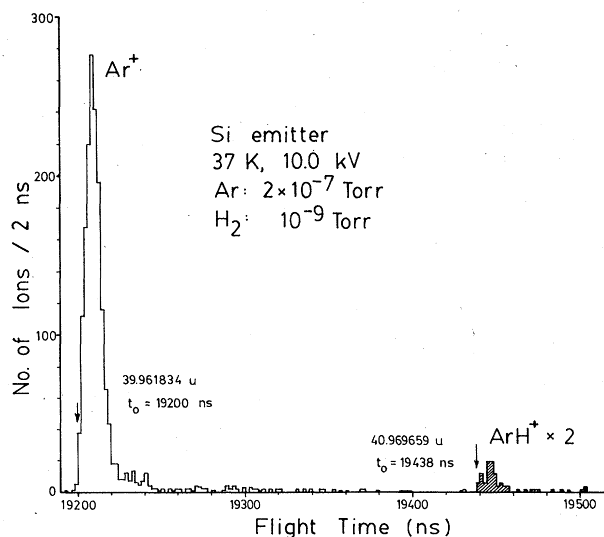

FIG. 19. Formation of ArH^+ in pulsed-laser field desorption from a silicon surface.

TABLE IV. Critical energy deficits of novel ions derived from the measured t_0 (4.2-m-long flight tube).

Ionic species Ionic mass (u) C (u/μs^2/kV)	V (kV)	t_0 (μs)	Measured $\Delta E_c^{(n)}/n$ (eV)	$\Delta E_c^{(n)}/n$ for metal ions (eV)
D_3^+	3.3	12.994	8.8	
6.041 756	3.7	12.270	9.8	
C =0.010 828 35	6.4	9.317	8.7	
	6.7	9.105	8.4	
	7.0	8.907	8.5	
			(Average: 8.8±0.5)	
$RhHe^{2+}$	8.7	23.810	11.8	10.9 (Rh^{2+})
53.453 228	9.2	23.152	11.5	
C =0.018 283 5	10.0	22.204	11.1	
			(Average: 11.5±0.3)	
$^{194}PtHe^{2+}$	11.0	28.813	11.9	11.4 (Pt^{2+})
98.982 092				
$^{195}PtHe^{2+}$		28.887	12.7	
99.483 145				
$^{196}PtHe^{2+}$		28.960	13.0	
99.983 226				
$^{198}PtHe^{2+}$		29.103	11.7	
100.984 692				
C =0.010 830 8			(Average: 12.3±0.5)	
ArH^+	10.0	19.438	~13.3±1.0	
40.969 659				
N_2H^+	9.0	17.238	~10.5±1.0	
29.013 424				
C =0.010 828 26				

proved by using an electronic timer of subnanosecond time resolution and a pulsed laser of a few picoseconds pulse width. Both these units are now commercially available. Only when the resolution is improved by a factor of ~10, accurate data of the higher ionization energies of heavy metal atoms and the binding energy, as well as the ionization energy of atomic clusters, can be derived from a critical-energy-deficit measurement.

ACKNOWLEDGMENTS

This work was supported by the National Science Foundation under Grant No. NSF-DMR-8217119. The author would also like to thank Y. Liou, S. B. McLane, T. J. Kinkus, and H. F. Liu for their help in some of the experimental preparations.

[1]R. Gomer, *Field Emission and Field Ionization* (Harvard University Press, Cambridge, Massachusetts, 1961).
[2]E. W. Müller and T. T. Tsong, *Field Ion Microscopy, Principles and Applications* (Elsevier, New York, 1969); Prog. Surf. Sci. **4**, 1 (1973).
[3]T. T. Tsong and T. J. Kinkus, Phys. Rev. B **29**, 529 (1984).
[4]T. T. Tsong, Y. Liou, and S. B. McLane, Rev. Sci. Instrum. **55**, 1246 (1984).
[5]T. T. Tsong, W. A. Schmidt, and O. Frank, Surf. Sci. **65**, 109 (1977); N. Ernst, G. Bozdesh, and J. H. Block, Int. J. Mass Spectrom. Ion Phys. **28**, 33 (1978).
[6]T. T. Tsong, S. B. McLane, and T. J. Kinkus, Rev. Sci. Instrum. **53**, 1442 (1982).
[7]C. M. Lederer and V. S. Shirley, *Table of Isotopes*, 7th ed. (Wiley, New York, 1978); A. H. Wapstra and K. Bos, At. Data Nucl. Data Tables **19**, 177 (1977).
[8]M. G. Inghram and R Gomer, J. Chem. Phys. **22**, 1279 (1954).
[9]T. T. Tsong and E. W. Müller, J. Chem. Phys. **41**, 3279 (1964).
[10]A. J. Jason, Phys. Rev. **156**, 266 (1967).
[11]G. R. Hanson and M. G. Inghram, Surf. Sci. **55**, 29 (1976).
[12]T. T. Tsong, J. H. Block, M. Nagasaka, and B. Viswanathan, J. Chem. Phys. **65**, 2469 (1976).
[13]D. S. Boudreaux and P. H. Cutler, Surf. Sci. **5**, 230 (1966).
[14]D. G. Brandon, Surf. Sci. **3**, 1 (1965); T. T. Tsong, *ibid.* **10**,

102 (1968); **70**, 211 (1978).
[15]R. Haydock and D. R. Kingham, Phys. Rev. Lett. **44**, 1520 (1980); D. R. Kingham, Surf. Sci. **116**, 273 (1982).
[16]W. Drachsel, Th. Jentsch, and J. H. Block, in *Proceedings of the 29th International Field Emission Symposium,* edited by H. O. Andren and H. Norden (Almqvist and Wiksell, Stockholm, 1982), p. 299.
[17]G. L. Kellogg, Appl. Surf. Sci. **11-12**, 186 (1982).
[18]C. E. Moore, *Ionization Potentials and Ionization Limits Derived from the Analysis of Optical Spectra,* Natl. Bur. Stand (U.S.) Reference Data Series No. NSRDS-NBS34 (U.S G.P.O. Washington, D.C. 1970).
[19]G. L. Kellogg and T. T. Tsong, J. Appl. Phys. **51**, 1184 (1980)
[20]K. Sattler, S. Mühlbach, O. Echt, P. Pfau, and E. Recknagel Phys. Rev. Lett. **47**, 160 (1981).
[21]T. T. Tsong, Surf. Sci. **81**, 28 (1979); **85**, 1 (1979).
[22]M. Hotokk, T. Kinsted, P. Pyykko, and Bo Roos, Mol. Phys **52**, 23 (1984).